Induction Machine Parameterization from Limited Transient Data using Convex Optimization

Ajay Pratap Yadav, *Student Member, IEEE,* Ramtin Madani, *Member, IEEE,* Navid Amiri, *Student Member, IEEE,* Juri Jatskevich, *Fellow, IEEE,* and Ali Davoudi, *Senior Member, IEEE*

***Abstract*—This paper identifies the parameters of an induction machine using limited and non-intrusive observations of available input voltages, stator currents, and the rotor speed. Parameter extraction is formulated as a non-convex estimation problem, which is then relaxed to a convex conic optimization problem. While the resulting relaxation could exhibit a satisfactory performance, there might be cases where the solution of convex relaxation fails to satisfy the dynamic equations of the machine. This is remedied through a local search approach initiated using the solution obtained from the relaxed problem. The proposed method is experimentally verified on a squirrel-cage induction machine with missing measured data. Using the measured signals as the benchmark, time-domain transients produced by the parameters estimated using the proposed method show almost 20% better match compared to time-domain transients produced by the parameters obtained via conventional testing.**

***Index Terms*—Conic relaxation, convex optimization, induction machine, parameter estimation, system identification.**

I. Introduction

Accurate machine characterization is needed for drive design and control, diagnostics and condition monitoring, controller/hardware-in-the-loop applications. Given that induction machines constitute a significant portion of loads in the grid, proper machine characterization is crucial to analysis of power system dynamics [1]. Mismatch between the actual and estimated parameter sets can deteriorate the drive performance [2]. Reliable data for most machines are not accessible, and excessive testing may not always be practical. Informative reviews on parameter identification of induction machines are presented in [3] and [4]. Conventionally, estimating parameters involves intrusive testing, e.g., IEEE Std. 112 [5]. One popular approach is to excite the machine with predetermined signals and monitor its response while maintaining a standstill rotor [6]–[8], which is suitable for 'self-commissioning' [9], [10]. In general, intrusive testings require isolated access to the machine, additional measurement equipment, and interruption of machine operation which might not be always feasible. For example, the locked-rotor test draws in large currents and could become impractical for some industrial setups. It is desirable to extract machine parameters from (preferably a single) transients during normal operation [11]. For example, [12] utilizes different portions of current and voltage transients to approximate conventional test scenarios.

A. P. Yadav and A. Davoudi were supported, in part, by the National Science Foundation under Grant 1509804. A. P. Yadav, R. Madani, and A. Davoudi are with the Department of Electrical Engineering, University of Texas at Arlington, TX, USA. Navid Amiri and Juri Jatskevich are with the Electrical and Computer Engineering Department, University of British Columbia, Vancouver, Canada.

The main parameters of interest for an induction machine are stator and rotor resistances, magnetizing inductance, stator and rotor leakage inductances, and mechanical inertia. Various methodologies exist for non-intrusive parameterization of induction machines, e.g., observer-based estimators [13], [14] or least-square regression [15], [16]. Observer-based methods, such as Kalman filters, can estimate system states and a subset of machine parameters using measured signals from the machine terminals. However, Kalman filters require proper initialization and noise covariance matrices [17]. [15] reformulates the machine model in terms of K-parameters, assuming slow-varying rotor speed, resulting in a standard linear least-square regression problem. [16] and [18] further extend this work to incorporate time-varying speed into the final regression problem. However, this involves estimating first- and second-order derivatives for certain current and flux-linkage terms, and are susceptible to noisy measurements. Usually, all these methods perform estimations using measurements of stator currents, input voltages, and rotor speed. [19] estimated machine parameters using only stator currents and voltages. This could, potentially, result in an ill-conditioned problem which would require an estimate for speed trajectory or an excellent initial guess, or could only offer a subset of parameters. Equivalent circuit model of an induction machine could be found using geometrical and electrical data [20], [21]. [22] employed finite-element model of an induction machine to extract its equivalent circuit model. [23] obtained the machine parameters from a high-fidelity magnetic-equivalent circuit model. Such methods require expert knowledge on the underlying complex models, manufacturing/fabrication errors, or material defects, and inherent the approximation present in the primary modeling effort.

One could employ nonlinear constraint optimization [24], [25] to minimize an objective function (usually, the norm of error between measured and predicted outputs) subject to machine model equations. A major challenge is the inherent non-convexity of the resulting optimization problem. Newton's method might not correctly converge without proper initialization. Various workarounds to tackle this limitation include (1) use of good initial conditions (from self-commissioning [10], [26] or conventional tests), (2) employing heuristics, e.g, enforcing box constraints on machine parameters [27], or (3) executing multiple optimization runs from different initial points [25]. Metaheuristic optimization techniques, e.g., genetic algorithms, can circumvent non-convexity albeit at a higher computational cost [28], [29]–[31]. In the context of power system estimation, [32] proposes a convex optimization

This article has been accepted for publication in a future issue of this journal, but has not been fully edited. Content may change prior to final publication. Citation information: DOI 10.1109/TIE.2021.3060668, IEEE Transactions on Industrial Electronics

approach to offer a good initial condition for the follow-up Newton's method. [23] has extracted parameters from magnetic equivalent circuit model of a synchronous machine using conic relaxation, assuming availability of all inputs and states, which is not a valid assumption for a physical machine.

We leverage the convex optimization framework to parameterize an induction machine using only limited samples of measurable signals. Herein, we assume a no-load operation and use data from start-up transients. The problem of non-convexity is tackled by formulating it in a higher-dimensional space and imposing conic constraints. Unlike original equations, the relaxed formulation can be solved efficiently using off-the-shelf solvers. To properly enforce machine dynamics, we feed the outcome of convex relaxation to a local search algorithm to obtain the desired near-optimal solution. Figure 1 provides an overview of the proposed approach, with its salient features summarized as follows:

- This method is non-intrusive; Parameters are identified using only limited samples of start-up transients.
- The proposed method does not require *a priori* knowledge of most machine parameters, which makes it suitable for refurbished or re-wounded machines.
- Machine parameters, including stator and rotor resistances, stator and rotor leakage inductances, magnetizing inductance, mechanical inertia, and the friction coefficient, are simultaneously identified.
- The proposed method reformulates a non-convex optimization problem into a tractable convex approximation. Detailed treatment of this transformation is provided. A penalized improvement of this convex relaxation is also discussed and verified using a test example.
- The proposed method is experimentally verified for an induction motor prototype, and is shown to converge even with missing points in available signals. Convergence is achieved with 80% of the measurement data. Robustness of the proposed method to noisy data is discussed.
- The set of machine parameters extracted by the proposed method are shown to result in a better match with the measured transients compared to the parameter set obtained by the conventional methods. Particularly, the proposed method has resulted in 12.5%-30% reduction in error when matching the stator currents, and 8.7% improvement when matching with the rotor speed transients.

II. Notations

Vectors and matrices are represented using bold lowercase and uppercase variables, respectively (e.g., $\boldsymbol{y}$ and $\boldsymbol{Y}$). The j^{th} element of vector $\boldsymbol{y}$ is y_j. $\boldsymbol{I}_n$ denotes a size n identity matrix. The notation $\text{diag}\{\boldsymbol{y}\}$ represents a diagonal matrix with the vector $\boldsymbol{y}$ forming the diagonal. For an $n\times n$ symmetric positive-definite matrix $\boldsymbol{Z}$ and the vector $\boldsymbol{y}\in\mathbb{R}^n$, the norm notation $\|\boldsymbol{y}\|_{\boldsymbol{Z}}$ denotes $\sqrt{\boldsymbol{y}^\top\boldsymbol{Z}\boldsymbol{y}}$. $\otimes$ stands for the Kronecker product. Symbol $\check{\cdot}$ represents the vectorization operator, i.e., $\check{\boldsymbol{\lambda}}\triangleq\left[\boldsymbol{\lambda}[1]^\top,\boldsymbol{\lambda}[2]^\top,\boldsymbol{\lambda}[3]^\top\ldots\right]^\top$. Set $\mathcal{A}$ is convex if, for every $\boldsymbol{y}_1,\boldsymbol{y}_2\in\mathcal{A}$ and any $\rho\in[0,1]$, $\rho\boldsymbol{y}_1+(1-\rho)\boldsymbol{y}_2\in\mathcal{A}$ [33].

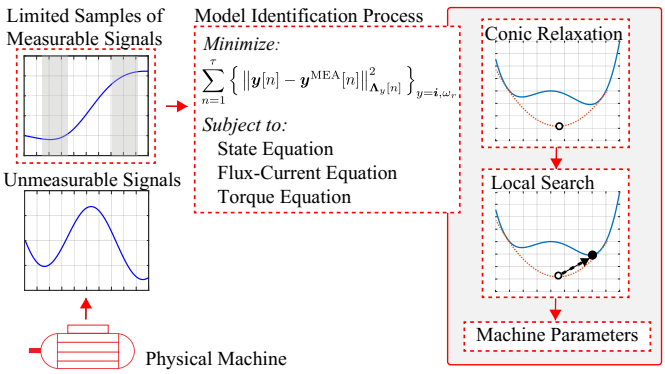

Fig. 1. Overview of the proposed model identification method.

III. Discrete-time Model of an Induction Machine

We present the classic dynamic model of an induction machine, and then adopt its discrete-time representation.

A. Machine Model

The induction machine model, in the arbitrary reference frame, is given by [34]

$$\frac{d\boldsymbol{\lambda}(t)}{dt} = \omega\Big[-\lambda_{ds}(t),\lambda_{qs}(t),-\lambda_{dr}(t),\lambda_{qr}(t)\Big]^\top + \omega_r(t)\Big[0,0,\lambda_{dr}(t),-\lambda_{qr}(t)\Big]^\top - \boldsymbol{R}\boldsymbol{i}(t)+\boldsymbol{v}(t), \quad (1a)$$

$$\boldsymbol{\lambda}(t) = \boldsymbol{L}\boldsymbol{i}(t), \quad (1b)$$

where $\boldsymbol{\lambda}(t)$, $\boldsymbol{i}(t)$, and $\boldsymbol{v}(t)$ are the vectors of flux linkages, currents, and voltages, respectively, defined as

$$\boldsymbol{\lambda}(t)\triangleq[\lambda_{qs}(t),\lambda_{ds}(t),\lambda_{qr}(t),\lambda_{dr}(t)]^\top, \quad (2a)$$

$$\boldsymbol{i}(t)\triangleq[i_{qs}(t),i_{ds}(t),i_{qr}(t),i_{dr}(t)]^\top, \quad (2b)$$

$$\boldsymbol{v}(t)\triangleq[v_{qs}(t),v_{ds}(t),v_{qr}(t),v_{dr}(t)]^\top. \quad (2c)$$

Subscripts qs, ds, qr, and dr denote q-axis stator, d-axis stator, q-axis rotor, and d-axis rotor terms, respectively. Zero-sequence terms are neglected in this balanced representation. $\boldsymbol{R}=\text{diag}\{[r_s,r_s,r_r,r_r]\}$ and $\boldsymbol{L}$ is

$$\boldsymbol{L}=\begin{bmatrix}L_s & 0 & L_m & 0\\ 0 & L_s & 0 & L_m\\ L_m & 0 & L_r & 0\\ 0 & L_m & 0 & L_r\end{bmatrix}. \quad (3)$$

ω represents the speed of the chosen reference frame, $\omega_r(t)$ is the rotor speed, r_s is the stator resistance, r_r is the rotor resistance, L_s is the stator self-inductance, L_r is the rotor self-inductance, and L_m is the magnetizing inductance. Stator and rotor leakage inductances can be obtained as $L_{ls}=L_s-L_m$ and $L_{lr}=L_r-L_m$, respectively. We assume an induction machine with shorted rotor bars, i.e., $v_{qr}=v_{dr}=0$.

The dynamics of the mechanical subsystem is [34]

$$\frac{d\omega_r(t)}{dt}=\frac{P}{2J}\left(T_e(t)-T_m(t)\right), \quad (4)$$

where P is the number of poles, J is the lumped mechanical inertia, T_e is the electromagnetic torque, and T_m is the

mechanical (load) torque. In this paper, we consider the start-up transient of an induction machine under free acceleration, where only friction torque is present. The equivalent friction torque can be found by subtracting the machine loss from the input power at the steady state, no-load operation. For simplicity, we assume that the friction coefficient has a linear relation with the rotor mechanical speed. The load torque is

$$T_m(t) = B\omega_r(t)/(P/2). \tag{5}$$

B is the total effective friction coefficient [11]. Electromagnetic torque is

$$T_e(t) = \frac{3}{4}P\left(\lambda_{ds}(t)i_{qs}(t) - \lambda_{qs}(t)i_{ds}(t)\right). \tag{6}$$

B. Discrete-time Representation

The machine model is discretized using the forward Euler method as it results in a simple explicit equations which eases the derivation of upcoming relaxation formulations. The discrete-time representation of (1), (4), and (6) become

$$\boldsymbol{\lambda}[n+1] = \boldsymbol{\lambda}[n] + \Delta T\Big(\omega\Big[-\lambda_{ds}[n], \lambda_{qs}[n], -\lambda_{dr}[n], \lambda_{qr}[n]\Big]^\top + \omega_r[n]\Big[0, 0, \lambda_{dr}[n], -\lambda_{qr}[n]\Big]^\top - \boldsymbol{R}\boldsymbol{i}[n] + \boldsymbol{v}[n]\Big), \tag{7a}$$

$$Q_w\omega_r[n+1] = Q_w\omega_r[n] + \frac{\Delta T}{2}\left(T_e[n] - \frac{2B\omega_r[n]}{P}\right), \tag{7b}$$

$$\boldsymbol{\lambda}[n] = \boldsymbol{L}\boldsymbol{i}[n], \tag{7c}$$

$$T_e[n] = \frac{3}{4}P\boldsymbol{\lambda}^\top[n]\Big[-i_{ds}[n], i_{qs}[n], 0, 0\Big]^\top. \tag{7d}$$

$n \in \mathcal{T}$ represents a time horizon with $\mathcal{T} \triangleq \{1, 2, 3, \ldots, \tau\}$, and ΔT is the sampling time interval. The variable $Q_w \triangleq J/P$ is defined to ensure that (7b) remains of degree two (quadratic), which will be helpful in the upcoming convex relaxation formulations. Note that P is a known constant.

IV. Parameter Extraction Procedure

Let $\boldsymbol{i}^{\text{MEA}}[n]$ and $\omega_r^{\text{MEA}}[n]$ denote the values of measured currents and rotor speeds, respectively, for $n \in \mathcal{T}$. Let $\mathcal{S}$ denote the set of different discrete-time horizons such as $\mathcal{T}$. The parameter identification problem is formulated as a weighted least-square optimization that minimizes the mismatch between predicted state variables in the discrete-time model (7) and the measured signals over $\mathcal{S}$,

minimize

$$\sum_{n\in\mathcal{S}} \left\|\text{diag}\{\boldsymbol{\iota}[n]\}\left(\boldsymbol{i}[n] - \boldsymbol{i}^{\text{MEA}}[n]\right)\right\|_{\boldsymbol{\Lambda}}^2 + \gamma\iota_\omega[n]\left(\omega_r[n] - \omega_r^{\text{MEA}}[n]\right)^2 \tag{8a}$$

subject to

$$\boldsymbol{\lambda}[n+1] = \boldsymbol{\lambda}[n] + \Delta T\Big(\omega\Big[-\lambda_{ds}[n], \lambda_{qs}[n], -\lambda_{dr}[n], \lambda_{qr}[n]\Big]^\top + \omega_r[n]\Big[0, 0, \lambda_{dr}[n], -\lambda_{qr}[n]\Big]^\top - \text{diag}\{[r_s, r_s, r_r, r_r]\}\,\boldsymbol{i}[n] + \boldsymbol{v}[n]\Big), \tag{8b}$$

$$Q_w\omega_r[n+1] = Q_w\omega_r[n] + \frac{\Delta T}{2}\left(T_e[n] - \frac{2B\omega_r[n]}{P}\right), \tag{8c}$$

$$\boldsymbol{\lambda}[n] = L_m\Big[i_{qr}[n], i_{dr}[n], i_{qs}[n], i_{ds}[n]\Big]^\top + \text{diag}\left\{[L_s, L_s, L_r, L_r]\right\}\boldsymbol{i}[n], \tag{8d}$$

$$T_e[n] = \frac{3}{4}P\boldsymbol{\lambda}^\top[n]\Big[-i_{ds}[n], i_{qs}[n], 0, 0\Big]^\top, \tag{8e}$$

variables

$$\left\{\boldsymbol{\lambda}[n], \boldsymbol{i}[n] \in \mathbb{R}^4, T_e[n], \omega_r[n] \in \mathbb{R}\right\}_{n\in\mathcal{S}},$$
$$r_s, r_r, L_s, L_r, L_m, Q_w, B \in \mathbb{R}.$$

$\boldsymbol{\Lambda} = \text{diag}\{[\alpha_1, \alpha_2, \alpha_3, \alpha_4]\}$ and γ contain non-negative weights to normalize current and speed terms, respectively. $\boldsymbol{\iota}[n] \in \{0, 1\}^4$ and $\iota_w[n] \in \{0, 1\}$ represent binary flags indicating the availability of the n^{th} data sample. Since rotor-side currents are hard to measure, it is reasonable to assume that $\iota_3[n] = \iota_4[n] = 0$ (corresponding to the rotor currents), and $\iota_1[n] = \iota_2[n] = 1$ (corresponding to the stator currents). Similarly, $\iota_w[n]$ is 1 or 0 depending upon the availability of speed measurement. The objective function (8a) represents the mismatch between the measured signals and the transients predicted by the estimated parameter set. The objective function denotes the sum of squared residuals (same as a least-squares regression). The equality constraints (8b) – (8e) reflect the discrete-time machine model (7a) – (7d). The induction machine model presented in (1), (4), and (6) are reflected within the optimization formulation. The unknown variables in the optimization problem (8) are separately listed below the constraints for convenience. The optimization problem (8a) – (8e) solves for flux linkages $\boldsymbol{\lambda}$, currents $\boldsymbol{i}$, torque T_e, and speed ω_r in $\mathcal{S}$, as well as the parameters $(r_s, r_r, L_s, L_r, L_m, Q_w, B)$, while minimizing the objective function, subject to machine dynamics. Measured data for stator currents (i_{qs} and i_{ds}), input voltage ($\boldsymbol{v}$), and rotor speed (ω_r), and the number of poles, P, are assumed known.

Observe that due to the the absence of rotor-side measurements, the estimation problem (8a) – (8e) suffers from solution ambiguity [35]. This is obvious from rotor-side flux linkage and current relations (see (7c)), where the expression $L_r i_{qr}$ (or $L_r i_{dr}$) can take identical values for different L_r and i_{qr} (or i_{dr}) in absence of rotor-side current measurements. To resolve this, we assume that the ratio L_s/L_r is known. It should be noted that if the NEMA design letter is known for the machine, the ratio L_s/L_r can be obtained from IEEE Std 112 [5], [36]. Inspired by [15], [16], [18], we assume $L_s/L_r = 1$. Note that any other known L_s/L_r ratio would would not affect the optimization process.

The optimization problem (8a) – (8e) is non-convex because of the following bilinear terms:

- $\omega_r\lambda_{qr}$, $\omega_r\lambda_{dr}$ and $r_s i_{qs}$, $r_s i_{ds}$, $r_r i_{qr}$, $r_r i_{dr}$ in (8b);
- $Q_w\omega_r$ and $B\omega_r$ in (8c);
- $L_s i_{qs}$, $L_s i_{ds}$, $L_r i_{qr}$, $L_r i_{dr}$ and $L_m i_{qr}$, $L_m i_{dr}$, $L_m i_{qs}$, $L_m i_{ds}$ in (8d);
- $\lambda_{qs} i_{ds}$ and $\lambda_{ds} i_{qs}$ in (8e).

Problem of non-convexity makes the optimization problem hard to solve, and standard tools, such as Newton's method, might not converge to the right solution without good initialization. In the following section, we transform this problem into a convex optimization formulation which could be solved in polynomial time using off-the-shelf solvers [33], [37].

V. Conic Relaxation and Numerical Search

To remedy the presence of non-convex bilinear terms, we introduce additional variables (lifting) and employ conic

relaxation to derive a convex optimization formulation for the problem (8a) – (8e).

A. Lifting

Non-convexity due to nonlinear terms (e.g., $\omega_r\lambda_{dr}$ and $r_s i_{qs}$) can be addressed by variable substitution. As a result, the objective function (8a) and constraints (8b) – (8e) can be rewritten as linear (convex) functions of variables in (8a) – (8e) and newly-defined auxiliary variables. This process is known as *lifting* in which the original optimization problem is cast into a higher dimensional space and the entire non-convexity is captured in the definition of auxiliary variables.

For every $n \in \mathcal{S}$, define the following additional variables

$$\boldsymbol{f}[n] \triangleq \omega_r[n]\ \Big[0, 0, \lambda_{dr}[n], -\lambda_{qr}[n]\Big]^\top, \tag{9a}$$
$$\boldsymbol{g}[n] \triangleq \operatorname{diag}\{[r_s, r_s, r_r, r_r]\}\,\boldsymbol{i}[n], \tag{9b}$$
$$\boldsymbol{h}[n] \triangleq L_s\boldsymbol{i}[n], \tag{9c}$$
$$\boldsymbol{z}[n] \triangleq L_m\Big[i_{qr}[n], i_{dr}[n], i_{qs}[n], i_{ds}[n]\Big]^\top, \tag{9d}$$
$$\boldsymbol{y}[n] \triangleq \Big[\lambda_{qs}[n]i_{ds}[n], \lambda_{ds}[n]i_{qs}[n], 0, 0\Big]^\top, \tag{9e}$$
$$\theta[n] \triangleq Q_w\omega_r[n], \qquad \phi[n] \triangleq B\omega_r[n], \tag{9f}$$
$$\bar{\boldsymbol{\lambda}}[n] \triangleq \operatorname{diag}\{\boldsymbol{\lambda}[n]\}\boldsymbol{\lambda}[n], \qquad \bar{\boldsymbol{i}}[n] \triangleq \operatorname{diag}\{\boldsymbol{i}[n]\}\boldsymbol{i}[n], \tag{9g}$$
$$\bar{\omega}_r[n] \triangleq \omega_r^2[n], \qquad \bar{T}_e[n] \triangleq T_e^2[n]. \tag{9h}$$

Define

$$\bar{r}_s \triangleq r_s^2, \quad \bar{r}_r \triangleq r_r^2, \quad \bar{Q}_w \triangleq Q_w^2, \tag{9i}$$
$$\bar{L}_m \triangleq L_m^2, \quad \bar{L}_s \triangleq L_s^2, \quad \bar{B} \triangleq B^2. \tag{9j}$$

There are two new sets of variables in above formulation: Those like $\boldsymbol{f}[n]$ that represent the non-convex terms, and those like $\bar{r}_s$ that denote squared variable. The need for such formulations will become clear in what follows. The optimization problem (8a) – (8e) can now be reformulated in terms of the auxiliary variables (9a) – (9j). However, additional constraints need to be included in the optimization problem to account for (9a) – (9j). A standard approach in convex optimization to represent bilinear expressions is using matrix equalities [23]. For example, $g_1[n] = r_s i_{qs}[n]$ in (9b) can be enforced as

$$\begin{bmatrix} \bar{r}_s & g_1[n] \\ g_1[n] & \bar{i}_1[n] \end{bmatrix} = \begin{bmatrix} r_s \\ i_{qs}[n] \end{bmatrix}\begin{bmatrix} r_s \\ i_{qs}[n] \end{bmatrix}^\top. \tag{10}$$

Expressing (9a) – (9j) as matrix equalities is helpful as they can be easily convexified. Variables such as $\bar{r}_s$ that denote squared variable are used to enforce equality conditions. Hence, problem (8a) – (8e) can now be reformulated as

minimize

$$\sum_{n\in\mathcal{S}} \boldsymbol{\iota}^\top[n]\boldsymbol{\Lambda}\Big(\bar{\boldsymbol{i}}[n] + \operatorname{diag}\{\boldsymbol{i}^{\text{MEA}}[n]\}(\boldsymbol{i}^{\text{MEA}}[n] - 2\boldsymbol{i}[n])\Big) + \gamma\iota_w[n]\Big(\bar{\omega}_r[n] - 2\,\omega_r^{\text{MEA}}[n]\omega_r[n] + \omega_r^{\text{MEA}}[n]^2\Big) \tag{11a}$$

subject to

$$\boldsymbol{\lambda}[n+1] = \boldsymbol{\lambda}[n] + \Delta T\Big(\omega\Big[-\lambda_{ds}[n], \lambda_{qs}[n], -\lambda_{dr}[n], \lambda_{qr}[n]\Big]^\top + \boldsymbol{f}[n] - \boldsymbol{g}[n] + \boldsymbol{v}[n]\Big), \tag{11b}$$

$$\theta[n+1] = \theta[n] + \frac{\Delta T}{2}\Big(T_e[n] - \frac{2\phi[n]}{P}\Big), \tag{11c}$$
$$\boldsymbol{\lambda}[n] = \boldsymbol{z}[n] + \boldsymbol{h}[n], \tag{11d}$$
$$T_e[n] = \frac{3P}{4}(y_2[n] - y_1[n]), \tag{11e}$$

$$\begin{bmatrix} \bar{\omega}_r[n] & (-1)^k f_k[n] \\ (-1)^k f_k[n] & \bar{\lambda}_{7-k}[n] \end{bmatrix} = \begin{bmatrix} -\omega_r[n] \\ \lambda_{7-k}[n] \end{bmatrix}\begin{bmatrix} -\omega_r[n] \\ \lambda_{7-k}[n] \end{bmatrix}^\top,$$
$$f_{5-k}[n] = 0, \qquad k = 3, 4. \tag{11f}$$

$$\begin{bmatrix} \bar{r}_s & g_k[n] \\ g_k[n] & \bar{i}_k[n] \end{bmatrix} = \begin{bmatrix} r_s \\ i_k[n] \end{bmatrix}\begin{bmatrix} r_s \\ i_k[n] \end{bmatrix}^\top, \qquad k = 1, 2. \tag{11g}$$
$$\begin{bmatrix} \bar{r}_r & g_k[n] \\ g_k[n] & \bar{i}_k[n] \end{bmatrix} = \begin{bmatrix} r_r \\ i_k[n] \end{bmatrix}\begin{bmatrix} r_r \\ i_k[n] \end{bmatrix}^\top, \qquad k = 3, 4. \tag{11h}$$

$$\begin{bmatrix} \bar{L}_s & h_k[n] \\ h_k[n] & \bar{i}_k[n] \end{bmatrix} = \begin{bmatrix} L_s \\ i_k[n] \end{bmatrix}\begin{bmatrix} L_s \\ i_k[n] \end{bmatrix}^\top, \qquad k = 1, 2, 3, 4. \tag{11i}$$

$$\begin{bmatrix} \bar{L}_m & z_k[n] \\ z_k[n] & \bar{i}_{k+2}[n] \end{bmatrix} = \begin{bmatrix} L_m \\ i_{k+2}[n] \end{bmatrix}\begin{bmatrix} L_m \\ i_{k+2}[n] \end{bmatrix}^\top, \qquad k = 1, 2. \tag{11j}$$
$$\begin{bmatrix} \bar{L}_m & z_k[n] \\ z_k[n] & \bar{i}_{k-2}[n] \end{bmatrix} = \begin{bmatrix} L_m \\ i_{k-2}[n] \end{bmatrix}\begin{bmatrix} L_m \\ i_{k-2}[n] \end{bmatrix}^\top, \qquad k = 3, 4. \tag{11k}$$

$$\begin{bmatrix} \bar{\lambda}_k[n] & y_k[n] \\ y_k[n] & \bar{i}_{3-k}[n] \end{bmatrix} = \begin{bmatrix} \lambda_k[n] \\ i_{3-k}[n] \end{bmatrix}\begin{bmatrix} \lambda_k[n] \\ i_{3-k}[n] \end{bmatrix}^\top,$$
$$y_{2+k}[n] = 0, \qquad k = 1, 2. \tag{11l}$$

$$\begin{bmatrix} \bar{Q}_w & \theta[n] \\ \theta[n] & \bar{\omega}_r[n] \end{bmatrix} = \begin{bmatrix} Q_w \\ \omega_r[n] \end{bmatrix}\begin{bmatrix} Q_w \\ \omega_r[n] \end{bmatrix}^\top,$$
$$\begin{bmatrix} \bar{B} & \phi[n] \\ \phi[n] & \bar{\omega}_r[n] \end{bmatrix} = \begin{bmatrix} B \\ \omega_r[n] \end{bmatrix}\begin{bmatrix} B \\ \omega_r[n] \end{bmatrix}^\top, \tag{11m}$$

variables

$$\{\boldsymbol{\lambda}[n], \bar{\boldsymbol{\lambda}}[n], \boldsymbol{i}[n], \bar{\boldsymbol{i}}[n], \boldsymbol{f}[n], \boldsymbol{g}[n], \boldsymbol{h}[n], \boldsymbol{z}[n], \boldsymbol{y}[n] \in \mathbb{R}^4\}_{n\in\mathcal{S}},$$
$$\{T_e[n], \bar{T}_e[n], \omega_r[n], \bar{\omega}_r[n], \theta[n], \phi[n] \in \mathbb{R}\}_{n\in\mathcal{S}},$$
$$r_s, \bar{r}_s, r_r, \bar{r}_r, L_s, \bar{L}_s, L_m, \bar{L}_m, Q_w, \bar{Q}_w, B, \bar{B} \in \mathbb{R}.$$

The optimization problem (11a) – (11m) is equivalent to (8a) – (8e). The objective function (11a) and constraints (11b) – (11e) are now expressed as linear equations using auxiliary variables to achieve convexification. The updated objective function (11a) is formulated as an algebraic expansion of (8a). Considering the assumption $L_s/L_r = 1$, variable L_r is replaced by L_s in the problem formulation. Matrix equalities (11f) – (11m) enforce (9a) – (9j). However, problem (11a) – (11m) is still non-convex due to these matrix equalities (11f) – (11m). In the following subsection, these equality conditions are relaxed which make the optimization problem convex.

B. Conic Relaxation

Relaxation aims to formulate a convex approximation of a non-convex optimization problem. Such a formulation is favorable because its every minimum is a global minimum that can be readily obtained. Usually, relaxation is achieved by eliminating or modifying the constraints that lead to non-convexity [33]. For the problem (11a) – (11m), relaxed formu-

This article has been accepted for publication in a future issue of this journal, but has not been fully edited. Content may change prior to final publication. Citation information: DOI 10.1109/TIE.2021.3060668, IEEE Transactions on Industrial Electronics

lation can be obtained by transforming all matrix equalities in (11f) – (11m) to matrix inequalities as shown in the following.

Definition 1. *Define $\mathcal{C}$ as the set of vectors $\mathbf{c} \in \mathbb{R}^5$ that satisfy*

$$\begin{bmatrix} c_1 & c_3 \\ c_3 & c_2 \end{bmatrix} \succeq \begin{bmatrix} c_4 \\ c_5 \end{bmatrix} \begin{bmatrix} c_4 \\ c_5 \end{bmatrix}^\top. \tag{12}$$

It is straightforward to observe that $\mathcal{C}$ is a convex set [33].

minimize

$$\sum_{n\in\mathcal{S}} \boldsymbol{\iota}^\top[n]\boldsymbol{\Lambda}\left(\bar{\boldsymbol{i}}[n] + \mathrm{diag}\{\boldsymbol{i}^{\mathrm{MEA}}[n]\}(\boldsymbol{i}^{\mathrm{MEA}}[n] - 2\boldsymbol{i}[n])\right) + \gamma\iota_w[n]\left(\bar{\omega}_r[n] - 2\,\omega_r^{\mathrm{MEA}}[n]\omega_r[n] + \omega_r^{\mathrm{MEA}}[n]^2\right) \tag{13a}$$

subject to

Machine model equations: (11b) – (11e) (13b)

$$\left[\bar{\omega}_r[n], \bar{\lambda}_{7-k}[n], (-1)^k f_k[n], -\omega_r[n], \lambda_{7-k}[n]\right]^\top \in \mathcal{C}$$

$$f_{5-k}[n] = 0, \qquad k=3,4. \tag{13c}$$

$$\left[\bar{r}_s, \bar{i}_k[n], g_k[n], r_s, i_k[n]\right]^\top \in \mathcal{C}, \qquad k=1,2.$$

$$\left[\bar{r}_r, \bar{i}_k[n], g_k[n], r_r, i_k[n]\right]^\top \in \mathcal{C}, \qquad k=3,4. \tag{13d}$$

$$\left[\bar{L}_s, \bar{i}_k[n], h_k[n], L_s, i_k[n]\right]^\top \in \mathcal{C}, \qquad k=1,2,3,4. \tag{13e}$$

$$\left[\bar{L}_m, \bar{i}_{k+2}[n], z_k[n], L_m, i_{k+2}[n]\right]^\top \in \mathcal{C}, \qquad k=1,2.$$

$$\left[\bar{L}_m, \bar{i}_{k-2}[n], z_k[n], L_m, i_{k-2}[n]\right]^\top \in \mathcal{C}, \qquad k=3,4. \tag{13f}$$

$$\left[\bar{\lambda}_k[n], \bar{i}_{3-k}[n], y_k[n], \lambda_k[n], i_{3-k}[n]\right]^\top \in \mathcal{C},$$

$$y_{2+k}[n] = 0, \qquad k=1,2. \tag{13g}$$

$$\left[\bar{Q}_w, \bar{\omega}_r[n], \theta[n], Q_w, \omega_r[n]\right]^\top \in \mathcal{C},$$

$$\left[\bar{B}, \bar{\omega}_r[n], \phi[n], B, \omega_r[n]\right]^\top \in \mathcal{C}, \tag{13h}$$

$$\bar{r}_s \geq r_s^2, \qquad \bar{r}_r \geq r_r^2, \qquad \bar{L}_s \geq L_s^2, \tag{13i}$$

$$\bar{L}_m \geq L_m^2, \quad \bar{Q}_w \geq Q_w^2, \quad \bar{B} \geq B^2 \tag{13j}$$

$$\bar{\boldsymbol{\lambda}}[n] \geq \mathrm{diag}\{\boldsymbol{\lambda}[n]\}\boldsymbol{\lambda}[n], \tag{13k}$$

$$\bar{\boldsymbol{i}}[n] \geq \mathrm{diag}\{\boldsymbol{i}[n]\}\boldsymbol{i}[n], \tag{13l}$$

$$\bar{\omega}_r[n] \geq \omega_r^2[n] \tag{13m}$$

$$\bar{T}_e[n] \geq T_e^2[n]. \tag{13n}$$

variables

$$\left\{\boldsymbol{\lambda}[n], \bar{\boldsymbol{\lambda}}[n], \boldsymbol{i}[n], \bar{\boldsymbol{i}}[n], \boldsymbol{f}[n], \boldsymbol{g}[n], \boldsymbol{h}[n], \boldsymbol{z}[n], \boldsymbol{y}[n] \in \mathbb{R}^4\right\}_{n\in\mathcal{S}},$$

$$\left\{T_e[n], \bar{T}_e[n], \omega_r[n], \bar{\omega}_r[n], \theta[n], \phi[n] \in \mathbb{R}\right\}_{n\in\mathcal{S}},$$

$$r_s, \bar{r}_s, r_r, \bar{r}_r, L_s, \bar{L}_s, L_m, \bar{L}_m, Q_w, \bar{Q}_w, B, \bar{B} \in \mathbb{R}.$$

(13c) – (13n) implicitly impose the matrix equalities (11f) – (11m). (13c) – (13n) are same as (11f) – (11m) except for the equality/inequality condition. A new notation using $\mathcal{C}$ is used for compactness. If the solution to the relaxed problem (13a) – (13n) satisfies (11f) – (11m) (probably unlikely), then the relaxation is declared as exact [33]. Otherwise, the obtained solution is infeasible for the problem (8a) – (8e). To assess the solution obtained from conic relaxation, we solve (13a) – (13n) for the startup transient of an induction machine. We consider a simulated case study where the relaxed problem is solved under different scenarios. The machine model used in the numerical simulation is constructed using the parameters obtained via conventional test as seen in Table I. The machine model is simulated with zero initial conditions and with the input voltage of 220 V (line-to-line). First, to establish a benchmark, rotor currents are *intentionally* assumed to be available. We then consider the realistic scenario that rotor currents are unavailable. Figure 2a shows the estimated currents $\boldsymbol{i}$, speed ω_r, and torque T_e (part of the optimization solution) for a scenario when the rotor currents are available with $\boldsymbol{\Lambda} = \mathrm{diag}\{[0.1, 0.1, 0.1, 0.1]\}$ and $\gamma = 0.1$. The result obtained from conic relaxation is near optimal as evident from the estimated waveforms. However, the absence of rotor current measurements (with $\boldsymbol{\Lambda} = \mathrm{diag}\{[0.1, 0.1, 0, 0]\}$ and $\gamma = 0.1$), leads to poor estimates for rotor currents and torque (see Figure 2b). (13a) – (13n) is a convex approximation to the original problem in (8a) – (8e), leading to an approximate solution in Figure 2b.

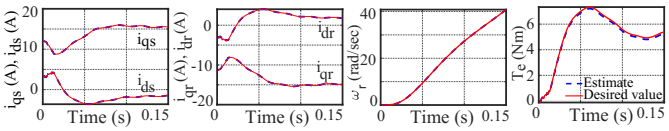

(a) Estimates from conic relaxation (13a) – (13n) using rotor currents.

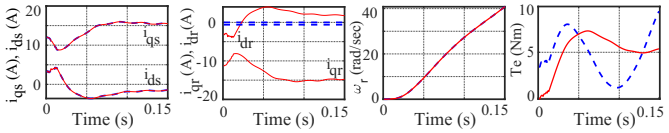

(b) Estimates from conic relaxation (13a) – (13n) without rotor currents.

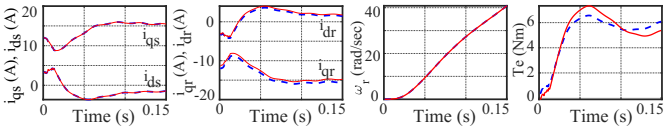

(c) Estimates from penalized conic relaxation (13a) – (13n) without rotor currents.

Fig. 2. Assessment of the estimates obtained from conic relaxation.

C. Incorporating Penalty

The solution from the conic relaxation can be further improved by incorporating penalty terms into the objective function [38]. Let $\hat{i}_{qr}$ and $\hat{i}_{dr}$ denote rough guesses for q-axis and d-axis rotor currents. Therefore, one can augment the objective function (13a) with the penalty term

$$\kappa = \sum_{n\in\mathcal{S}} \eta_{i_{qr}}(\bar{i}_{qr}[n] - 2\hat{i}_{qr}[n]i_{qr}[n] + \hat{i}_{qr}^2[n]) + \eta_{i_{dr}}(\bar{i}_{dr}[n] - 2\hat{i}_{dr}[n]i_{dr}[n] + \hat{i}_{dr}^2[n]). \tag{14}$$

$\eta_{i_{qr}}$ and $\eta_{i_{dr}}$ are user-defined non-negative gains with $\bar{i}_{qr} \triangleq i_{qr}^2$ and $\bar{i}_{dr} \triangleq i_{dr}^2$. The penalty term in (14) incentivizes

This article has been accepted for publication in a future issue of this journal, but has not been fully edited. Content may change prior to final publication. Citation information: DOI 10.1109/TIE.2021.3060668, IEEE Transactions on Industrial Electronics

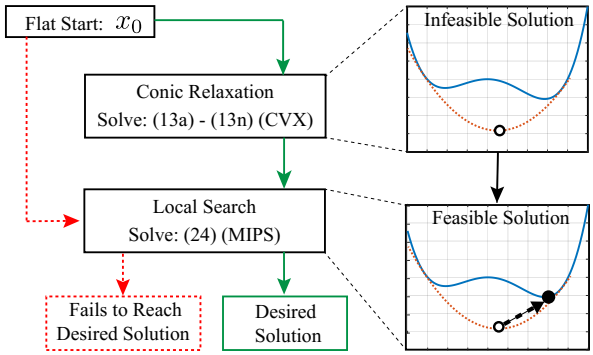

Fig. 3. Overview of the two-step solution for the estimation problem in (8).

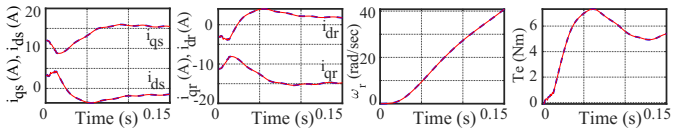

Fig. 4. Local search results for the example in Fig. 2, which is initialized with the solution of the penalized conic relaxation in Fig. 2c.

the optimization solver to search around the neighborhood of guessed rotor currents. The penalty term (14) is a convex reformulation for $\eta_{i_{qr}}(i_{qr}[n]-\hat{i}_{qr}[n])^2+\eta_{i_{dr}}(i_{dr}[n]-\hat{i}_{dr}[n])^2$. A decent guess for rotor currents can be $\hat{i}_{qr}[n] \approx -i_{qs}[n]$ and $\hat{i}_{dr}[n] \approx -i_{ds}[n]$ during the startup [19]. Similarly, at the steady state, $\hat{i}_{qr}[n] \approx 0$ and $\hat{i}_{dr}[n] \approx 0$. Figure 2c shows the results for the relaxed problem (13a) – (13n) when the objective function (13a) is augmented with the penalty term (14). Penalization significantly improves the results for the relaxed problem (with $\boldsymbol{\Lambda} = \text{diag}\{[0.1, 0.1, 0, 0]\}$, $\gamma = 0.1$, and $\eta_{i_{qr}} = \eta_{i_{dr}} = 1$).

D. Local Search

As discussed in Section V-B, the solution to the relaxed optimization problem (13a) – (13n) could be infeasible for the original problem (8a) – (8e). It can, however, serve as an excellent initial condition to a local search algorithm [32]. To solve the estimation problem using an iterative Newton's method, we need to formulate the Karush-Kuhn-Tucker (KKT) conditions [33]. By defining the optimization variable as

$$\boldsymbol{x} \triangleq \left[\check{\boldsymbol{\lambda}}^\top, \check{\boldsymbol{i}}^\top, \check{\boldsymbol{T}}_e^\top, \check{\boldsymbol{\omega}}_r^\top, L_s, L_m, r_s, r_r, Q_w, B\right]^\top, \tag{15}$$

the equality constraint (8b) – (8e) can then be cast as

$$\boldsymbol{\mathcal{E}}(\boldsymbol{x}) \triangleq [\boldsymbol{\mathcal{E}_1}(\boldsymbol{x})^\top\ \boldsymbol{\mathcal{E}_2}(\boldsymbol{x})^\top\ \boldsymbol{\mathcal{E}_3}(\boldsymbol{x})^\top\ \boldsymbol{\mathcal{E}_4}(\boldsymbol{x})^\top]^\top = \boldsymbol{0}, \tag{16}$$

where

$$\boldsymbol{\mathcal{E}_1}(\boldsymbol{x}) \triangleq (\boldsymbol{K}_1 - \boldsymbol{K}_2)\check{\boldsymbol{\lambda}} - \Delta T\Big((\text{diag}\{\boldsymbol{K}_4\check{\boldsymbol{\omega}}_r\}\otimes \boldsymbol{I}_4)\boldsymbol{N}_1\boldsymbol{K}_2\check{\boldsymbol{\lambda}} + \omega\boldsymbol{N}_2\boldsymbol{K}_2\check{\boldsymbol{\lambda}} - (\boldsymbol{I}_{\tau-1}\otimes\boldsymbol{R})\boldsymbol{K}_2\check{\boldsymbol{i}} + \boldsymbol{K}_2\check{\boldsymbol{v}}\Big), \tag{17a}$$

$$\boldsymbol{\mathcal{E}_2}(\boldsymbol{x}) \triangleq Q_w\boldsymbol{K}_3\check{\boldsymbol{\omega}}_r - \boldsymbol{K}_4\big(Q_w\check{\boldsymbol{\omega}}_r + \frac{\Delta T}{2}(\check{\boldsymbol{T}}_e - \frac{2B}{P}\check{\boldsymbol{\omega}}_r)\big), \tag{17b}$$

$$\boldsymbol{\mathcal{E}_3}(\boldsymbol{x}) \triangleq \check{\boldsymbol{\lambda}} - (\boldsymbol{I}_\tau \otimes \text{diag}\{[L_s, L_s, L_s, L_s]\})\check{\boldsymbol{i}} - L_m\boldsymbol{N}_3\check{\boldsymbol{i}}, \tag{17c}$$

$$\boldsymbol{\mathcal{E}_4}(\boldsymbol{x}) \triangleq \check{\boldsymbol{T}}_e - \frac{3P}{4}\text{diag}\{(\boldsymbol{I}_\tau \otimes \boldsymbol{d}_2^\top)\check{\boldsymbol{\lambda}}\}(\boldsymbol{I}_\tau \otimes \boldsymbol{d}_1^\top)\check{\boldsymbol{i}} + \frac{3P}{4}\text{diag}\{(\boldsymbol{I}_\tau \otimes \boldsymbol{d}_1^\top)\check{\boldsymbol{\lambda}}\}(\boldsymbol{I}_\tau \otimes \boldsymbol{d}_2^\top)\check{\boldsymbol{i}}. \tag{17d}$$

$\boldsymbol{K}_1 \triangleq [\boldsymbol{0}_{4(\tau-1)\times 4}, \boldsymbol{I}_{4(\tau-1)}]$, $\boldsymbol{K}_2 \triangleq [\boldsymbol{I}_{4(\tau-1)}, \boldsymbol{0}_{4(\tau-1)\times 4}]$, $\boldsymbol{K}_3 \triangleq [\boldsymbol{0}_{\tau-1}, \boldsymbol{I}_{\tau-1}]$, and $\boldsymbol{K}_4 \triangleq [\boldsymbol{I}_{\tau-1}, \boldsymbol{0}_{\tau-1}]$ and

$$\mathbf{N}_1 \triangleq \boldsymbol{I}_{\tau-1} \otimes (\boldsymbol{d}_3\boldsymbol{d}_4^\top - \boldsymbol{d}_4\boldsymbol{d}_3^\top), \tag{18a}$$

$$\mathbf{N}_2 \triangleq \boldsymbol{I}_{\tau-1} \otimes (-\boldsymbol{d}_1\boldsymbol{d}_2^\top + \boldsymbol{d}_2\boldsymbol{d}_1^\top - \boldsymbol{d}_3\boldsymbol{d}_4^\top + \boldsymbol{d}_4\boldsymbol{d}_3^\top), \tag{18b}$$

$$\mathbf{N}_3 \triangleq \boldsymbol{I}_\tau \otimes (\boldsymbol{d}_1\boldsymbol{d}_3^\top + \boldsymbol{d}_2\boldsymbol{d}_4^\top + \boldsymbol{d}_3\boldsymbol{d}_1^\top + \boldsymbol{d}_4\boldsymbol{d}_2^\top). \tag{18c}$$

$\boldsymbol{x}$ denotes the concatenated form of the optimization variable. Symbol $\check{\cdot}$ represents the vectorization operator (see notations). $\boldsymbol{\mathcal{E}_1}(\boldsymbol{x})$, $\boldsymbol{\mathcal{E}_2}(\boldsymbol{x})$, $\boldsymbol{\mathcal{E}_3}(\boldsymbol{x})$, and $\boldsymbol{\mathcal{E}_4}(\boldsymbol{x})$ are the vectorized form of machine model (7). Variables $\mathbf{K}_1 - \mathbf{K}_4$ and $\mathbf{N}_1 - \mathbf{N}_3$ are defined to achieve vectorization. $(\boldsymbol{d}_1, \boldsymbol{d}_2, \boldsymbol{d}_3, \boldsymbol{d}_4)$ are the standard basis of $\mathbb{R}^4$. One can formulate the Jacobian matrix $\boldsymbol{J}(\boldsymbol{x})$ for the constraints (17a) – (17d) in the form of (19). In (19), $\nabla_{\{\cdot\}}$ denotes the derivative with respect to the subscript variable, e.g., $\nabla_{\check{\boldsymbol{\lambda}}}\mathcal{E}_1$ is the derivative of $\mathcal{E}_1$ with respect to $\check{\boldsymbol{\lambda}}$. Additionally, the Lagrangian function $\mathcal{L}$ of the optimization problem (8a) – (8e) can be cast as

$$\mathcal{L}(\boldsymbol{x};\boldsymbol{\nu}) \triangleq (\check{\boldsymbol{i}} - \check{\boldsymbol{i}}^{\text{MEA}})^\top\big(\text{diag}\{\check{\boldsymbol{\iota}}\}(\boldsymbol{I}_\tau \otimes \boldsymbol{\Lambda})\big)(\check{\boldsymbol{i}} - \check{\boldsymbol{i}}^{\text{MEA}}) + \gamma(\check{\boldsymbol{\omega}}_r - \check{\boldsymbol{\omega}}_r^{\text{MEA}})^\top\text{diag}\{\check{\boldsymbol{\iota}}_\omega\}(\check{\boldsymbol{\omega}}_r - \check{\boldsymbol{\omega}}_r^{\text{MEA}}) + \boldsymbol{\nu}^\top\boldsymbol{\mathcal{E}}(\boldsymbol{x}), \tag{20}$$

where $\boldsymbol{\nu}$ is the vector of Lagrange multipliers, $\check{\boldsymbol{i}}^{\text{MEA}}$ and $\check{\boldsymbol{\omega}}_r^{\text{MEA}}$ denote vectorized current and speed measurements. The gradient of $\mathcal{L}$ with respect to $\boldsymbol{x}$ can be formulated as

$$\boldsymbol{G}(\boldsymbol{x};\boldsymbol{\nu}) \triangleq 2 \times \Big[\boldsymbol{0}, \Big(\big(\text{diag}\{\check{\boldsymbol{\iota}}\}(\boldsymbol{I}_\tau \otimes \boldsymbol{\Lambda})\big)(\check{\boldsymbol{i}} - \check{\boldsymbol{i}}^{\text{MEA}})\Big)^\top, \boldsymbol{0}, \gamma\Big(\text{diag}\{\check{\boldsymbol{\iota}}_\omega\}(\check{\boldsymbol{\omega}}_r - \check{\boldsymbol{\omega}}_r^{\text{MEA}})\Big)^\top, \boldsymbol{0}\Big] + \boldsymbol{\nu}^\top\boldsymbol{J}(\boldsymbol{x}). \tag{21}$$

Finally, the Hessian of $\mathcal{L}$ is

$$\boldsymbol{H}(\boldsymbol{x};\boldsymbol{\nu}) \triangleq \begin{bmatrix} \boldsymbol{H}_{11} & \boldsymbol{H}_{12} \\ \boldsymbol{H}_{12}^\top & \boldsymbol{0} \end{bmatrix}, \tag{22}$$

where

$$\boldsymbol{H}_{11} \triangleq \begin{bmatrix} \boldsymbol{0} & \frac{\partial^2\mathcal{L}}{\partial\check{\boldsymbol{\lambda}}\partial\check{\boldsymbol{i}}} & \boldsymbol{0} & \frac{\partial^2\mathcal{L}}{\partial\check{\boldsymbol{\lambda}}\partial\check{\boldsymbol{\omega}}_r} \\ \frac{\partial^2\mathcal{L}}{\partial\check{\boldsymbol{i}}\partial\check{\boldsymbol{\lambda}}} & \frac{\partial^2\mathcal{L}}{\partial\check{\boldsymbol{i}}^2} & \boldsymbol{0} & \boldsymbol{0} \\ \boldsymbol{0} & \boldsymbol{0} & \boldsymbol{0} & \boldsymbol{0} \\ \frac{\partial^2\mathcal{L}}{\partial\check{\boldsymbol{\omega}}_r\partial\check{\boldsymbol{\lambda}}} & \boldsymbol{0} & \boldsymbol{0} & \frac{\partial^2\mathcal{L}}{\partial\check{\boldsymbol{\omega}}_r^2} \end{bmatrix}, \tag{23a}$$

$$\boldsymbol{H}_{12} \triangleq \begin{bmatrix} \boldsymbol{0} & \boldsymbol{0} & \boldsymbol{0} & \boldsymbol{0} & \boldsymbol{0} & \boldsymbol{0} \\ \frac{\partial^2\mathcal{L}}{\partial\check{\boldsymbol{i}}\partial L_s} & \frac{\partial^2\mathcal{L}}{\partial\check{\boldsymbol{i}}\partial L_m} & \frac{\partial^2\mathcal{L}}{\partial\check{\boldsymbol{i}}\partial r_s} & \frac{\partial^2\mathcal{L}}{\partial\check{\boldsymbol{i}}\partial r_r} & \boldsymbol{0} & \boldsymbol{0} \\ \boldsymbol{0} & \boldsymbol{0} & \boldsymbol{0} & \boldsymbol{0} & \boldsymbol{0} & \boldsymbol{0} \\ \boldsymbol{0} & \boldsymbol{0} & \boldsymbol{0} & \boldsymbol{0} & \frac{\partial^2\mathcal{L}}{\partial\check{\boldsymbol{\omega}}_r\partial Q_w} & \frac{\partial^2\mathcal{L}}{\partial\check{\boldsymbol{\omega}}_r\partial B} \end{bmatrix}. \tag{23b}$$

Newton steps of the form

$$\begin{bmatrix} \Delta\boldsymbol{x} \\ \Delta\boldsymbol{\nu} \end{bmatrix} = -\begin{bmatrix} \boldsymbol{H}(\boldsymbol{x};\boldsymbol{\nu}) & \boldsymbol{J}(\boldsymbol{x})^\top \\ \boldsymbol{J}(\boldsymbol{x}) & \boldsymbol{0} \end{bmatrix}^{-1}\begin{bmatrix} \boldsymbol{G}(\boldsymbol{x};\boldsymbol{\nu})^\top \\ \boldsymbol{\mathcal{E}}(\boldsymbol{x}) \end{bmatrix}, \tag{24}$$

converge to a solution that meets the KKT optimality conditions. Figure 4 shows the results for the example presented in Figure 2, when the solution of the penalized conic relaxation (Fig. 2c) initializes a local search procedure. Figure 3 shows the steps needed to solve the estimation problem (8a) – (8e).

This article has been accepted for publication in a future issue of this journal, but has not been fully edited. Content may change prior to final publication. Citation information: DOI 10.1109/TIE.2021.3060668, IEEE Transactions on Industrial Electronics

$$\boldsymbol{J}(\boldsymbol{x}) = \begin{bmatrix} \nabla_{\check{\boldsymbol{\lambda}}}\mathcal{E}_1 & \nabla_{\check{\boldsymbol{i}}}\mathcal{E}_1 & \mathbf{0} & \nabla_{\check{\omega}_r}\mathcal{E}_1 & \mathbf{0} & \mathbf{0} & \nabla_{r_s}\mathcal{E}_1 & \nabla_{r_r}\mathcal{E}_1 & \mathbf{0} & \mathbf{0} \\ \mathbf{0} & \mathbf{0} & \nabla_{\check{T}_e}\mathcal{E}_2 & \nabla_{\check{\omega}_r}\mathcal{E}_2 & \mathbf{0} & \mathbf{0} & \mathbf{0} & \mathbf{0} & \nabla_{Q_w}\mathcal{E}_2 & \nabla_B\mathcal{E}_2 \\ \nabla_{\check{\boldsymbol{\lambda}}}\mathcal{E}_3 & \nabla_{\check{\boldsymbol{i}}}\mathcal{E}_3 & \mathbf{0} & \mathbf{0} & \nabla_{L_s}\mathcal{E}_3 & \nabla_{L_m}\mathcal{E}_3 & \mathbf{0} & \mathbf{0} & \mathbf{0} & \mathbf{0} \\ \nabla_{\check{\boldsymbol{\lambda}}}\mathcal{E}_4 & \nabla_{\check{\boldsymbol{i}}}\mathcal{E}_4 & \nabla_{\check{T}_e}\mathcal{E}_4 & \mathbf{0} & \mathbf{0} & \mathbf{0} & \mathbf{0} & \mathbf{0} & \mathbf{0} & \mathbf{0} \end{bmatrix} \tag{19}$$

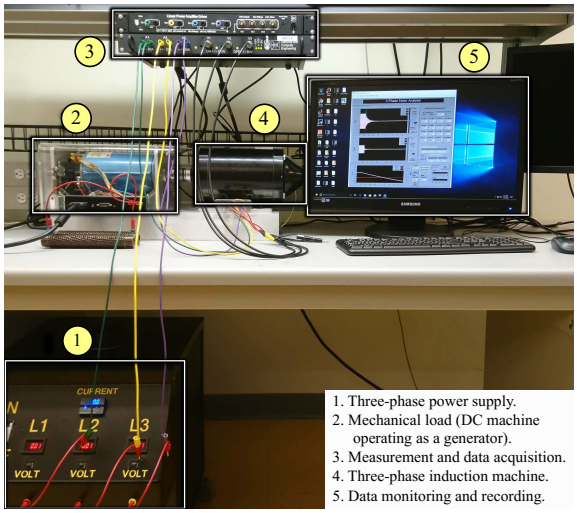

Fig. 5. Hardware setup used to measure machine transients and characteristics.

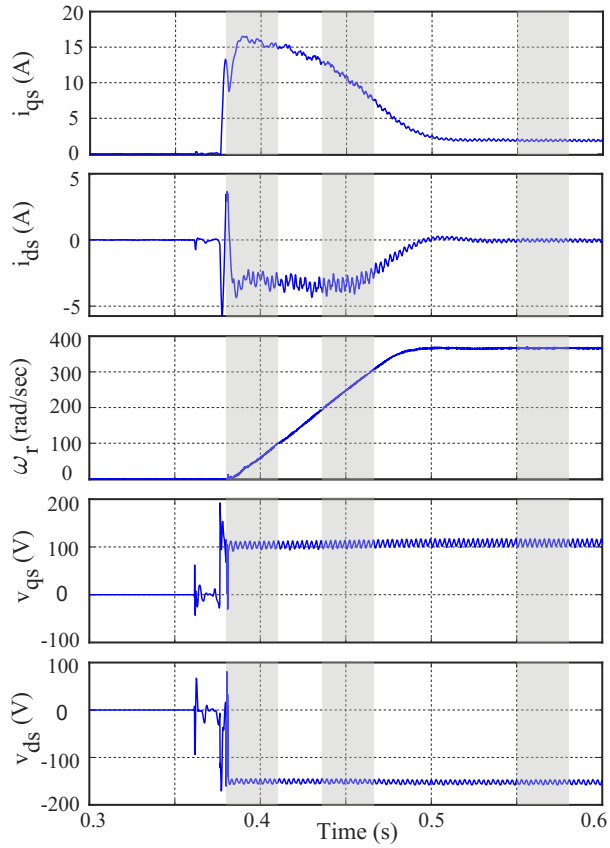

Fig. 6. Measured startup transients for the underlying induction machine. The highlighted portion of the transients are used for parameter identification.

VI. Experimental Studies

A. Numerical and Experimental Setups

The numerical studies are performed on a workstation using Windows 10 equipped with quad-core Intel® Core™ i7-6700 with 32 GB RAM. The relaxed optimization problem (13a) – (13n) is solved using the SDPT3 4.0 [39] solver in the CVX [37] environment on MATLAB 2019a. MATPOWER Interior Point Solver (MIPS) [40] version 1.3.1 performs the local search. MIPS solves (24) using the formulations of objective function and equality constraints (8a) – (8e), Jacobian matrix (19), Hessian matrix (22), and the solution of the relaxed optimization problem (13a) – (13n) as an initial condition. The termination tolerances for the MIPS solver, namely, `gradtol`, `feastol`, `comptol`, and `costtol` are selected as 10^{-8}, 10^{-8}, 10^{-6}, and 10^{-6}, respectively. The maximum iteration count is set to 50.

Figure 5 shows the experimental setup used for measurement acquisition. The four-pole motor is excited with a voltage of 220 V (line-to-line). The measured data is demonstrated in Fig. 6. For comparison, machine parameters have also been identified through standard intrusive characterization tests [5]. These conventional tests include dc stator resistance measurements, locked rotor test (used for identifying rotor resistance along with stator and rotor leakage inductances), no-load test (used for identifying magnetizing inductance), no-load deceleration test (used for identifying total lumped inertia of the machine and dynamometer), and no-load startup test (used for identifying start-up impedance of the machine).

B. Parameter Extraction from Measurement

Parameters such as leakage inductance and inertia are more dominant during transients, whereas magnetizing inductance has a prominent effect at the steady state. Hence, limited data from both acceleration and steady-state phases of the measured waveforms are used for the model identification procedure. Sampling time of 100 μs is used in the measured data shown in Fig. 6. The highlighted portions of the data is used for parameter extraction. Synchronous reference frame is chosen for the machine model with $\omega = 120\pi$. The non-negative weights for the relaxed problem (13a) – (13n) and the local search (8a) – (8e) are $\boldsymbol{\Lambda} = \text{diag}\{[0.1, 0.1, 0, 0]\}$ and $\gamma = 0.1$, with binary flags as $\boldsymbol{\iota} = [1, 1, 0, 0]^\top$ and $\iota_w = 1$. While choosing $\boldsymbol{\Lambda}$ and γ, one should note that (1) larger gain implies higher priority for the optimization solver, and (2) gains can be used to normalize the order of terms in the objective function. For example, $\boldsymbol{\Lambda} = \text{diag}\{[1, 1, 0, 0]\}$ and $\gamma = 1$ or $\boldsymbol{\Lambda} = \text{diag}\{[0.01, 0.01, 0, 0]\}$ and $\gamma = 0.01$ are also viable options. The gains for penalty terms in (14) are set as $\eta_{i_{qr}} = \eta_{i_{dr}} = 1$. The optimization problem (13a) – (13n), with the penalty term (14), is first solved. The outcome of

TABLE I
MACHINE PARAMETERS EXTRACTED USING THE CONVENTIONAL TESTS AND THE PROPOSED METHOD

Methodology	L_s (H)	L_m (H)	L_r (H)	r_s (Ω)	r_r (Ω)	J (kg.m^2)	B (N.m.s/rad)	Objective fn (8a)
Proposed Method	0.3149	0.3040	0.3149	4.50	3.45	0.0041	0.0089	648.3
Conventional Tests	0.3207	0.3087	0.3207	4.52	3.23	0.0037	-	1235.2

this relaxation is then used as an initial point for the local search (24) (see Fig. 3). A single run of convex relaxation takes approximately 185 seconds (including all overheads) on average. Local search concludes within 60 seconds. Table I compares the machine parameters estimated by the proposed method against parameters extracted using conventional tests. In addition to resistances, inductances, and inertia terms, we could estimate the friction coefficient as well. Table I also lists the values of objective function (8a) that, for the proposed method, is almost half of that predicted by parameters obtained from conventional tests. Since rotor current measurements are not available, (8a) takes the following form

$$\sum_{n\in\mathcal{S}} \alpha_1\iota_1[n](i_{qs}[n]-i_{qs}^{\text{MEA}}[n])^2+\alpha_2\iota_2[n](i_{ds}[n]-i_{ds}^{\text{MEA}}[n])^2 \\ +\gamma\iota_\omega[n]\big(\omega_r[n]-\omega_r^{\text{MEA}}[n]\big)^2. \tag{25}$$

The aggregate value of (25) is attributed to individual mismatch expressions for stator currents (i_{qs} and i_{ds}) and rotor speed (ω_r). For the proposed method, the contribution due to the first expression in (25) is about 10.5, the second expression is 14.4, and the last expression is 623.4. For parameters obtained from conventional tests, respective expressions contribute about 27.3 (mismatch in i_{qs}), 34.0 (mismatch in i_{ds}), and 1173.9 (mismatch in ω_r). The absolute value of (25) depends on user-defined coefficients α_1, α_2, and γ. Therefore, one should consider the relative improvement in the value of the objective function obtained by the proposed method, as shown in the last column of Table I. Moreover, as opposed to multiple interruptive and intrusive tests needed in the conventional approach, our method extracts machine parameters from measured data obtained during the machine's normal operation.

Two dynamic models built using two sets of machine parameters, one extracted using the proposed method and another obtained via conventional methods, are considered. Figures 7 and 8 compare the stator currents and speed waveforms obtained from simulating the machine models using the two sets of parameters listed in Table I. Figure 9 shows the trajectories of both stator and rotor flux linkages and currents in the *qd*-axis. The machine model is simulated with zero initial conditions. Parameters obtained from the proposed method result in an excellent fit to the measured data as evident from Fig. 7. Figure 8 shows a zoomed-in view of a portion of stator current in Figure 7. It is evident that the time-domain transients predicted by the parameters obtained by the proposed method match better with the measured signal compared to transients predicted by the parameters obtained using the conventional methods. This fit can be quantified using metrics like the root-

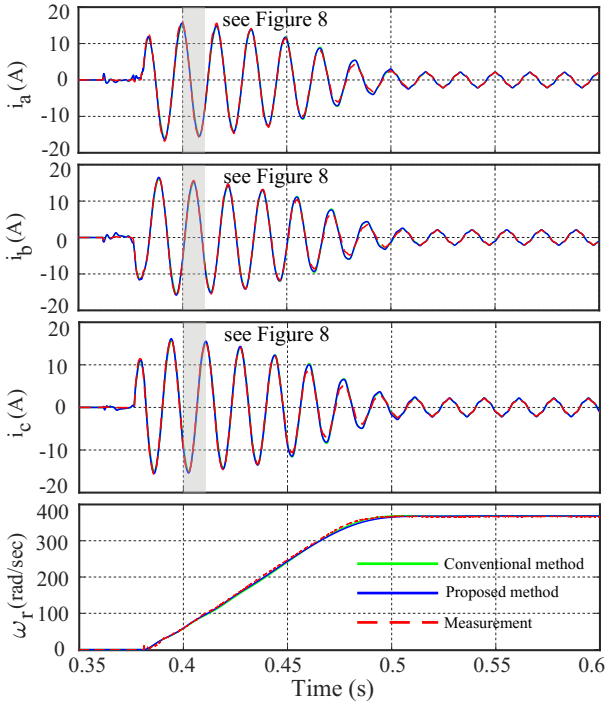

Fig. 7. Estimated parameters listed in Table I are used to simulate the induction machine model from zero initial conditions. The resulting current and speed waveforms are compared against measured data.

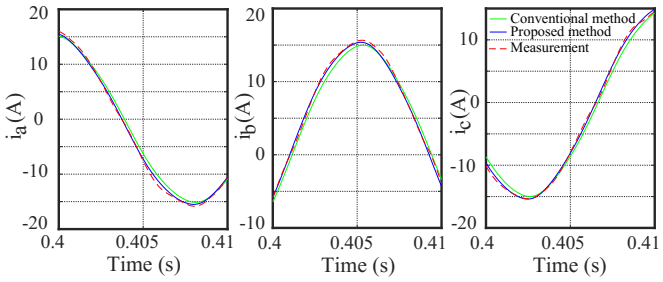

Fig. 8. Zoomed-in version of the highlighted portions of Fig. 7. We can observe a better match between the waveforms predicted by the estimated parameters with measurements.

mean-square error (RMSE) or the 2-norm error defined as

$$\text{RMSE} = \sqrt{\frac{1}{N}\sum_{i=1}^{N}(x_i^{\text{MEA}} - x_i^{\text{EST}})^2}, \tag{26a}$$

$$\text{2-norm error} = \frac{\sqrt{\sum_{i=1}^{N}(x_i^{\text{MEA}} - x_i^{\text{EST}})^2}}{\sqrt{\sum_{i=1}^{N}(x_i^{\text{MEA}})^2}} \times 100. \tag{26b}$$

x_i^{EST} and x_i^{MEA} are the i^{th} samples of the estimated and measured signals, respectively. N denotes the number of samples considered. Table II lists RMSE and 2-norm error values while

This article has been accepted for publication in a future issue of this journal, but has not been fully edited. Content may change prior to final publication. Citation information: DOI 10.1109/TIE.2021.3060668, IEEE Transactions on Industrial Electronics

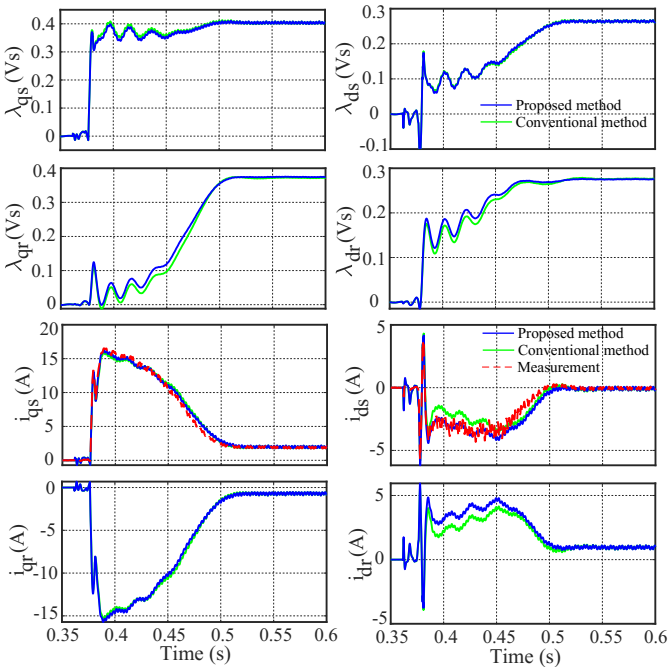

Fig. 9. Trajectories of *qd* flux linkages and currents obtained using the parameters listed in Table I. Stator currents are compared against measurements.

TABLE II
QUANTIFICATION OF THE MISMATCH AGAINST MEASUREMENT

Signal	RMSE		2-norm		Percentage Improved
	Proposed method	Conventional tests	Proposed method	Conventional tests	
i_a	0.433	0.625	6.847	9.882	30.7
i_b	0.455	0.520	7.188	8.216	12.5
i_c	0.441	0.593	7.076	9.514	25.6
ω_r	3.70	4.05	1.227	1.343	8.7
Average					19.3

comparing the two sets of machine waveforms against real measurements. Parameters extracted by the proposed method result in lower RMSE and 2-norm error as compared to the parameter obtained from conventional tests. Table II lists the percentage reduction in error values against parameters from conventional tests. RMSE reduces from 0.625 to 0.433 for the phase-a current, a 30% percent improvement. The RMSE for rotor speed has improved by more than 8%. On average, we see a 19.3% improvement in error. Percentage improvements in Table II are the same for both RMSE and 2-norm metrics.

C. Estimation with Missing Data Points

We now test the resilience of the proposed method against loss in measured data. We assume that indicators $\boldsymbol{\iota}[n]$ and $\iota_w[n]$ take the value 1 with a probability of 0.8, such that random data points for stator currents and rotor speed are flagged as unavailable in (8a) and (13a). This is implemented using the rand function (uniformly distributed pseudorandom numbers) in MATLAB. Figure 10 compares the estimated current and speed trajectories against the input measurements. Signal loss is shown by zeros along the time axis for illustration purposes (lost data are not necessarily zero in value). The optimization algorithm successfully reproduces the entire current trajectory along with machine parameters.

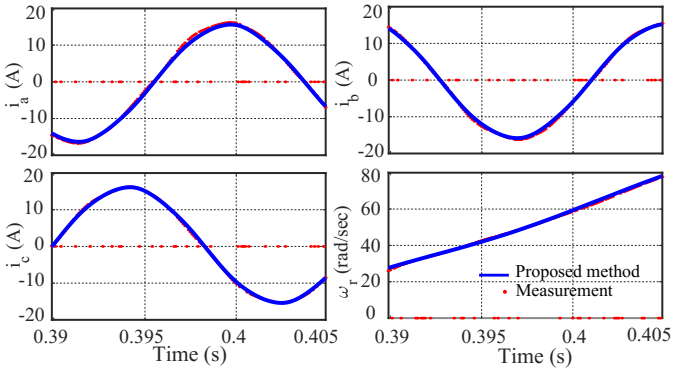

Fig. 10. Stator currents and rotor speed transients, considering lossy measurement, predicted by the estimated parameters versus input measurement. The red dots along the time-axis represent the instances of data loss.

TABLE III
PARAMETER SETS OBTAINED FROM NOISY DATA

Machine Parameters	0% noise	2% noise	5% noise
L_s	0.3207	0.3216	0.3193
L_m	0.3087	0.3096	0.3074
L_r	0.3207	0.3216	0.3193
r_s	4.52	4.57	4.38
r_r	3.23	3.18	3.27
J	0.0037	0.0036	0.0038
B	0.0089	0.0087	0.0085

D. Impact of Noisy Input Data

The machine model is first simulated assuming the parameters listed in Table I (conventional tests values) and, then, the resulting state transients are polluted with noise signals with zero mean and 2%/5% standard deviations. Figure 11 shows both the noise-free and distorted transients. Table III lists the parameters obtained under different noise scenarios. As seen, estimated parameters, in presence of noisy data, are in good agreement with those obtained from noise-free data. In practice, low-pass filtering effects of acquisition devices eliminate severe noisy data. Interested readers can refer to [41] for a detailed theoretical analysis on the impact of noise on the performance of conic relaxation equipped a weighted least squared estimator, and to [42], [43] for the treatment of process or measurement noise in estimation process.

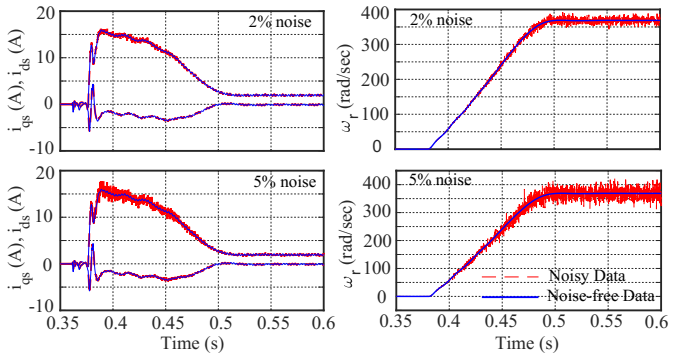

Fig. 11. Simulated machine transients polluted with different noise levels.

This article has been accepted for publication in a future issue of this journal, but has not been fully edited. Content may change prior to final publication. Citation information: DOI 10.1109/TIE.2021.3060668, IEEE Transactions on Industrial Electronics

TABLE IV
ESTIMATION RESULTS UNDER VARIOUS SAMPLING TIMES

Machine Parameters	$\Delta T = 50\ \mu s$	$\Delta T = 100\ \mu s$	$\Delta T = 200\ \mu s$	$\Delta T = 300\ \mu s$
L_s	0.3153	0.3149	0.3068	0.3412
L_m	0.3043	0.3040	0.2958	0.3300
L_r	0.3153	0.3149	0.3068	0.3412
r_s	4.51	4.50	4.44	4.68
r_r	3.44	3.45	3.52	3.26
J	0.0041	0.0041	0.0042	0.0040
B	0.0089	0.0089	0.0077	0.0091

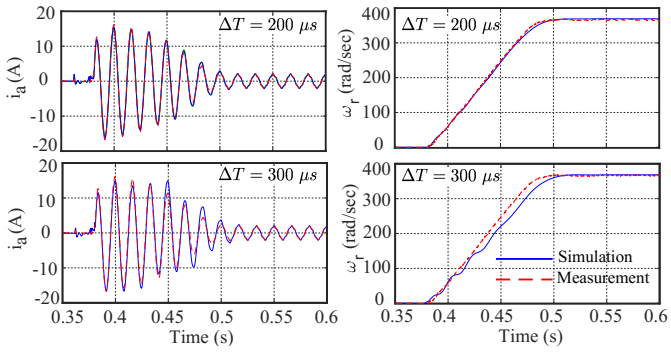

Fig. 12. Machine transients simulated under different ΔTs, with parameter sets obtained under those ΔTs, compared to hardware measurement.

E. Impact of Sampling Time

For a given time horizon of data, increasing sampling time interval ΔT reduces the number of data points used in the estimation process. On the other hand, ΔT should be sufficiently small to have fidelity with the original machine equations. Using available data from Figure 6, Table IV lists parameters extracted under different sampling time intervals. As ΔT is increased, estimated parameters start to deviate due to errors induced by the discretization process. Figure 12 compares the measured data against machine transients simulated using the parameters sets in the last two columns of Table IV (and their respective sampling times). Notice that, particularly, at ΔT=300μs, simulated transients clearly deviate from their measured counterparts.

VII. CONCLUSION

We extract the parameters of an induction machine in a non-intrusive manner using startup transients. The non-convex parameter identification problem is convexified using conic relaxation, whose output is transformed into an accurate solution for the machine dynamical equations using a local search. The proposed method is experimentally shown to identify machine parameters, even with intermittent losses in measured data. These parameters are shown to result in a better match with the measured signals compared to those obtained using conventional tests (nearly a 20% improvement in matching transient waveforms). Future research direction includes expanding this approach to more comprehensive machine models (e.g., with variable parameters).

REFERENCES

[1] P. Kundur, *Power system stability and control*. New York, USA: McGraw-Hill, 1994.

[2] H. A. Maksoud, S. M. Shaaban, M. S. Zaky, and H. Z. Azazi, "Performance and stability improvement of afo for sensorless im drives in low speeds regenerating mode," *IEEE Trans. Power Electron.*, vol. 34, no. 8, pp. 7812–7825, Aug. 2019.

[3] H. A. Toliyat, E. Levi, and M. Raina, "A review of RFO induction motor parameter estimation techniques," *IEEE Trans. Energy Convers.*, vol. 18, no. 2, pp. 271–283, Jun. 2003.

[4] S. A. Odhano, P. Pescetto, H. A. A. Awan, M. Hinkkanen, G. Pellegrino, and R. Bojoi, "Parameter identification and self-commissioning in AC motor drives: A technology status review," *IEEE Trans. Power Electron.*, vol. 34, no. 4, pp. 3603–3614, Apr. 2019.

[5] *IEEE Standard Test Procedure for Polyphase Induction Motors and Generators*, IEEE Std. 112-2017, 2018.

[6] L. Monjo, H. Kojooyan-Jafari, F. Corcoles, and J. Pedra, "Squirrel-cage induction motor parameter estimation using a variable frequency test," *IEEE Trans. Energy Conv.*, vol. 30, no. 2, pp. 550–557, Jun. 2015.

[7] J. Ruan and S. Wang, "A prediction error method-based self-commissioning scheme for parameter identification of induction motors in sensorless drives," *IEEE Trans. Energy Conv.*, vol. 30, no. 1, pp. 384–393, Mar. 2015.

[8] S. R. P. Reddy and U. Loganathan, "Offline recursive identification of electrical parameters of vsi-fed induction motor drives," *IEEE Trans. Power Electron.*, vol. 35, no. 10, pp. 10 711–10 719, Oct. 2020.

[9] S. Lee, A. Yoo, H. Lee, Y. Yoon, and B. Han, "Identification of induction motor parameters at standstill based on integral calculation," *IEEE Trans. Ind. Appl.*, vol. 53, no. 3, pp. 2130–2139, May 2017.

[10] M. Carraro and M. Zigliotto, "Automatic parameter identification of inverter-fed induction motors at standstill," *IEEE Trans. Ind. Electron.*, vol. 61, no. 9, pp. 4605–4613, Sep. 2014.

[11] J. Benzaquen, J. Rengifo, E. Albanez, and J. M. Aller, "Parameter estimation for deep-bar induction machines using instantaneous stator measurements from a direct startup," *IEEE Trans. Energy Convers.*, vol. 32, no. 2, pp. 516–524, Jun. 2017.

[12] S. Chiniforoosh, L. M. Vargas, L. Wang, and J. Jatskevich, "Online characterization procedure for induction machines using start-up and loading transients," in *Proc. IEEE Canada Elect. Power Conf.*, Vancouver, BC, Canada, 2008, pp. 1–5.

[13] P. Huynh, H. Zhu, and D. Aliprantis, "Non-intrusive parameter estimation for single-phase induction motors using transient data," in *Proc. IEEE Power & Energy Conf.*, Champaign, IL, USA, 2015, pp. 1–8.

[14] D. J. Atkinson, P. P. Acarnley, and J. W. Finch, "Observers for induction motor state and parameter estimation," *IEEE Trans. Ind. Appl.*, vol. 27, no. 6, pp. 1119–1127, Nov. 1991.

[15] J. Stephan, M. Bodson, and J. Chiasson, "Real-time estimation of the parameters and fluxes of induction motors," *IEEE Trans. Ind. Appl.*, vol. 30, no. 3, pp. 746–759, May 1994.

[16] H. Kojooyan-Jafari, L. Monjo, F. Corcoles, and J. Pedra, "Parameter estimation of wound-rotor induction motors from transient measurements," *IEEE Trans. Energy Conv.*, vol. 29, no. 2, pp. 300–308, Jun. 2014.

[17] F. Auger, M. Hilairet, J. M. Guerrero, E. Monmasson, T. Orlowska-Kowalska, and S. Katsura, "Industrial applications of the kalman filter: A review," *IEEE Trans. Ind. Electron.*, vol. 60, no. 12, pp. 5458–5471, Dec. 2013.

[18] Kaiyu Wang, J. Chiasson, M. Bodson, and L. M. Tolbert, "A nonlinear least-squares approach for identification of the induction motor parameters," *IEEE Trans. Autom. Control*, vol. 50, no. 10, pp. 1622–1628, Oct. 2005.

[19] S. R. Shaw and S. B. Leeb, "Identification of induction motor parameters from transient stator current measurements," *IEEE Trans. Ind. Electron.*, vol. 46, no. 1, pp. 139–149, Feb. 1999.

[20] A. Boglietti, A. Cavagnino, and M. Lazzari, "Computational algorithms for induction-motor equivalent circuit parameter determination - part i: Resistances and leakage reactances," *IEEE Trans. Ind. Electron.*, vol. 58, no. 9, pp. 3723–3733, Sep. 2011.

[21] ——, "Computational algorithms for induction motor equivalent circuit parameter determination - part ii: Skin effect and magnetizing characteristics," *IEEE Trans. Ind. Electron.*, vol. 58, no. 9, pp. 3734–3740, Sep. 2011.

[22] Z. Ling, L. Zhou, S. Guo, and Y. Zhang, "Equivalent circuit parameters calculation of induction motor by finite element analysis," *IEEE Trans. Magn.*, vol. 50, no. 2, pp. 833–836, Feb. 2014.

[23] A. P. Yadav, T. Altun, R. Madani, and A. Davoudi, "Macromodeling of electric machines from ab initio models," *IEEE Trans. Energy Convers.*, vol. 35, no. 2, pp. 908–916, Jun. 2020.

[24] M. Cirrincione, M. Pucci, G. Cirrincione, and G. Capolino, "Constrained minimization for parameter estimation of induction motors in saturated

and unsaturated conditions," *IEEE Trans. Ind. Electron.*, vol. 52, no. 5, pp. 1391–1402, Oct. 2005.
[25] L. Fagiano, M. Lauricella, D. Angelosante, and E. Ragaini, "Identification of induction motors using smart circuit breakers," *IEEE Trans. Control Syst. Technol.*, vol. 27, no. 6, pp. 2638–2646, Nov. 2019.
[26] Y. He, Y. Wang, Y. Feng, and Z. Wang, "Parameter identification of an induction machine at standstill using the vector constructing method," *IEEE Trans. Power Electron.*, vol. 27, no. 2, pp. 905–915, Feb. 2012.
[27] F. Duan, R. Zivanovic, S. Al-Sarawi, and D. Mba, "Induction motor parameter estimation using sparse grid optimization algorithm," *IEEE Trans. Ind. Informat.*, vol. 12, no. 4, pp. 1453–1461, Aug. 2016.
[28] K. S. Huang, Q. H. Wu, and D. R. Turner, "Effective identification of induction motor parameters based on fewer measurements," *IEEE Trans. Energy Convers.*, vol. 17, no. 1, pp. 55–60, Mar. 2002.
[29] Jong-Wook Kim and Sang Woo Kim, "Parameter identification of induction motors using dynamic encoding algorithm for searches (deas)," *IEEE Trans. Energy Conv.*, vol. 20, no. 1, pp. 16–24, Mar. 2005.
[30] D. Bhowmick, M. Manna, and S. K. Chowdhury, "Estimation of equivalent circuit parameters of transformer and induction motor from load data," *IEEE Trans. Ind. Appl.*, vol. 54, no. 3, pp. 2784–2791, May 2018.
[31] Z. Liu, H. Wei, X. Li, K. Liu, and Q. Zhong, "Global identification of electrical and mechanical parameters in pmsm drive based on dynamic self-learning pso," *IEEE Trans. Power Electron.*, vol. 33, no. 12, pp. 10 858–10 871, Dec. 2018.
[32] Y. Weng, Q. Li, R. Negi, and M. Ilic, "Semidefinite programming for power system state estimation," in *Proc. IEEE Power & Energy Soc. Gen. Meeting*, San Diego, CA, USA, 2012, pp. 1–8.
[33] S. Boyd and L. Vandenberghe, *Convex optimization*. Cambridge, U.K.: Cambridge University Press, 2004.
[34] P. Krause, O. Wasynczuk, S. D. Sudhoff, and S. Pekarek, *Analysis of electric machinery and drive systems*, 3rd ed. Piscataway, NJ, USA: IEEE Press, 2013.
[35] A. M. Alturas, S. M. Gadoue, B. Zahawi, and M. A. Elgendy, "On the identifiability of steady-state induction machine models using external measurements," *IEEE Trans. Energy Conv.*, vol. 31, no. 1, pp. 251–259, Mar. 2016.
[36] D. M. Reed, H. F. Hofmann, and J. Sun, "Offline identification of induction machine parameters with core loss estimation using the stator current locus," *IEEE Trans. Energy Convers.*, vol. 31, no. 4, pp. 1549–1558, Dec. 2016.
[37] M. Grant and S. Boyd. (2014, Mar.) CVX: Matlab software for disciplined convex programming, version 2.1. [Online]. Available: http://cvxr.com/cvx
[38] R. Madani, M. Kheirandishfard, J. Lavaei, and A. Atamturk, "Penalized semidefinite programming for quadratically-constrained quadratic optimization," *arXiv preprint arXiv:2004.14328*, Apr. 2020.
[39] R. H. Tütüncü, K. C. Toh, and M. J. Todd, "Solving semidefinite-quadratic-linear programs using SDPT3," *Mathematical Programming*, vol. 95, no. 2, pp. 189–217, Feb. 2003.
[40] R. D. Zimmerman and H. Wang. (2019, Jun.) MATPOWER interior point solver (MIPS) user's manual, version 1.3.1. [Online]. Available: https://matpower.org/docs/MIPS-manual-1.3.1.pdf
[41] R. Madani, J. Lavaei, and R. Baldick, "Convexification of power flow equations in the presence of noisy measurements," *IEEE Trans. Autom. Control*, vol. 64, no. 8, pp. 3101–3116, Aug. 2019.
[42] M. Iqbal, A. I. Bhatti, S. I. Ayubi, and Q. Khan, "Robust parameter estimation of nonlinear systems using sliding-mode differentiator observer," *IEEE Trans. Indust. Electron.*, vol. 58, no. 2, pp. 680–689, Feb. 2011.
[43] F. Alonge, F. D'Ippolito, and A. Sferlazza, "Sensorless control of induction-motor drive based on robust kalman filter and adaptive speed estimation," *IEEE Trans. Indust. Electron.*, vol. 61, no. 3, pp. 1444–1453, Mar. 2014.

Ajay Pratap Yadav received the Bachelor's and Master's degree in Electrical engineering from the Indian Institute of Technology Roorkee and Indian Institute of Technology Kanpur, in 2010 and 2014, respectively. He is currently pursuing his Ph.D. at the University of Texas at Arlington. His research interests include electric machine modeling, system identification, optimization, and microgrids.

Ramtin Madani received the Ph.D. degree in electrical engineering from Columbia University, New York, NY, USA, in 2015. He was a Postdoctoral Scholar with the Department of Industrial Engineering and Operations Research at University of California, Berkeley in 2016. He is an Assistant Professor with the Department of Electrical Engineering Department, University of Texas at Arlington, Arlington, TX, USA. His research interests include developing algorithms for optimization and control with applications in energy.

Navid Amiri (S'11 - M'19) received his B.Sc. and M.Sc. degrees in electrical engineering in the field of power and electrical machines from Isfahan University of Technology, Isfahan, Iran, in 2008 and 2011, and his Ph.D. degree in electrical and computer engineering in 2019 from the University of British Columbia, Vancouver, BC, Canada. He is currently a Postdoctoral Research Fellow in electrical and computer engineering department at the University of British Columbia. His research interests include numerically efficient modeling of electric machines, real-time simulation, electromechanical energy conversion systems, electric machine design, and power electronics.

Juri Jatskevich (M'99 - F'17) received the M.S.E.E. and the Ph.D. degrees in Electrical Engineering from Purdue University, West Lafayette IN, USA, in 1997 and 1999, respectively. Since 2002, he has been a faculty member at the University of British Columbia, Vancouver, Canada, where he is now a Professor in the Department of Electrical and Computer Engineering. His research interests include power electronic systems, electrical machines and drives, modeling and simulation of electromagnetic transients.

ALI DAVOUDI (S'04-M'11-SM'15) received his Ph.D. in Electrical and Computer Engineering from the University of Illinois, Urbana-Champaign, IL, USA, in 2010. He is currently a Professor in the Electrical Engineering Department, University of Texas, Arlington, TX, USA. He is an Associate Editor for the IEEE TRANSACTIONS ON POWER ELECTRONICS, and an Editor for the IEEE TRANSACTIONS ON ENERGY CONVERSION as well as IEEE POWER ENGINEERING LETTERS. His research interests include modeling, control, and optimization of power electronics systems.